

Investigation on time-dependent wetting behavior of Ni-Cu-P ternary coating

Jie Wang, Junpeng Liu, Nigel Neate, Mingwen Bai, Fang Xu, Tanvir Hussain, Colin Scotchford and Xianghui Hou*

Faculty of Engineering, University of Nottingham, University Park, Nottingham NG7 2RD, UK;

* Correspondence: xianghui.hou@nottingham.ac.uk; Tel: +44-115-95-13920

ABSTRACT

Hydrophobic metallic coatings have attracted increasing interest in the recent years due to their excellent mechanical durability. But the wetting behavior and hydrophobic mechanism of metallic coatings are far from clear. In this work, Ni-Cu-P ternary coatings with hierarchical structure were prepared on 304 stainless steel by electrodeposition method. The surface morphologies, phase compositions, and wetting behavior were studied systemically. Time-dependent wetting behaviour of Ni-Cu-P coatings had been clearly observed, and the surface of the as-deposited coatings changed from hydrophilic state to hydrophobic state after aging in ambient air. The related surface wetting mechanism was investigated with the assistance of plasma cleaning to study the possible surface adsorption contributing to the time-dependent wetting behavior. The variations of the surface species were analyzed using X-ray photoelectron spectroscopy (XPS), showing the composition change of both carbon and the oxygen. The atomic ratio of hydrocarbon on the Ni-Cu-P coating first increased from 78.7 % to 86.5 % when stored in ambient air and then decreased from 82.3 % to 65.9 % after the plasma cleaning treatment; while the variation of oxygen content was an opposite trend. The results indicated that the observed time-dependent wettability was a combined result of the adsorption of airborne hydrocarbon and the change of lattice oxygen on the coating surface.

Key Words: Wettability; airborne hydrocarbon; Hydrophobicity; Ni-Cu-P ternary alloy; Lattice oxygen; Electrodeposition.

1. Introduction

Hydrophobic surface is defined as a solid surface with static water contact angle higher than 90° and tends to repel water droplets. Because of the broad technological potentials, great attention has been paid [1, 2] on developing various hydrophobic coatings for a wide range of applications, such as self-cleaning [3, 4], anti-icing [5, 6], corrosion resistance [7], electro-wetting [8] and so on. There are two key factors influencing the surface hydrophobicity: surface topography, e.g. hierarchical micro/nanostructure [9] and surface energy determined by the material composition [10]. Among current hydrophobic coatings, various polymeric coating systems have been developed intensively and play the dominant position. But the limited durability of these polymeric coatings remains the biggest challenge [11], as they cannot survive long-termly in a harsh environment, which is a major restriction for their practical applications [1, 12].

In recent years, metallic-based hydrophobic surface and coatings have been attracting significant interests due to their outstanding mechanical durability and possible multifunctionalities. Wei et al prepared a Fe-based composite surface using electro-brush plating which exhibited excellent hydrophobicity, anti-corrosion performance and abrasion resistance [13]. Khorsand et al fabricated super-hydrophobic Ni–Co coatings that exhibited good chemical stability and long-term durability as well as the self-cleaning effect [14]. Vorobyev et al reported a hydrophobic multifunctional metal surface showing combined effects of self-cleaning, anti-biofouling, and self-sanitation by producing a hierarchical nano- and micro-structures with femtosecond laser pulses [15].

Among these metallic coatings, Ni-Cu-P ternary coating system is a promising candidate for practical hydrophobic applications because of its high mechanical properties [16] and anti-corrosion performance [17], etc. The anti-corrosion performance of Ni–Cu–P coatings are superior to common Ni-based coatings [18]. Ni-Cu-P coatings also possess improved anti-

friction and anti-wear performance, as compared with ordinary Ni-based coatings [19, 20]. The hydrophobic Ni-Cu-P ternary coatings have been preliminarily reported [21]. But its unusual feature of time-dependent wettability has not been discovered and the detailed surface wetting mechanism has yet to be studied. This work would not only help to establish an in-depth understanding of the surface chemistry towards the wettability of metallic coatings, but also inspire the R&D of the relevant applications. Materials with controllable wetting behaviours would have meaningful application prospects, for example, controlled transportation of fluids, tuneable wettability devices and so on [22, 23].

Electrodeposition is a convenient method to create micro/nanostructures metallic coatings which could be readily controlled by adjusting deposition parameters [24]. In the present work, Ni-Cu-P ternary coatings with hierarchical structure were prepared by electrodeposition methods. It was found that the surface of the as-deposited coatings changed from hydrophilic state to hydrophobic state after aging in ambient air. The time-dependent wetting behaviour of the Ni-Cu-P ternary coatings was investigated, for the aim to disclose the possible wetting mechanism, which is likely to be applicable to other metallic coatings.

2. Experimental

2.1 Materials

Nickel sulfate hexahydrate ($\text{NiSO}_4 \cdot 6\text{H}_2\text{O}$), copper sulfate pentahydrate ($\text{CuSO}_4 \cdot 5\text{H}_2\text{O}$), sodium dihydrogen phosphate (NaH_2PO_2), citric acid, sodium dodecyl sulfate (SDS) and sodium sulfate (Na_2SO_4) were obtained from Sigma-Aldrich (Dorset, UK). All of the chemicals were analytical grade reagents and used as received. 304 stainless steel (SS) plates were selected as the main substrates. High purity Nickel foil (99.96%) was used as the anode (Shenzhen Changsheng Telecom Technology Co. Ltd, China). Deionised water with a resistivity of $18.2 \text{ M}\Omega \cdot \text{cm}$ was used in the preparation of aqueous electrolyte.

2.2 Coating Preparation

Electrodeposition was performed using a DC power supply (1739 BK Precision, UK). The substrates were machined into 15mm × 15mm × 1mm square plates. Grit blasting was carried out using 220 grit white alumina before the coating preparation, to enhance the bonding between the coating and the substrate. Then the substrates were activated in diluted hydrochloric acid (HCl) solution and cleaned in the ultrasonic bath with deionized water for 10 min. The electrolyte consisted of 0.125 mol/L NiSO₄, 0.005 mol/L CuSO₄, 0.026 mol/L NaH₂PO₂, 0.05 mol/L citric acid and 0.12 g/L SDS. Na₂SO₄ (0.5 mol/L) was added to the electrolyte to enhance the solution ion strength. The pH value was adjusted to 5.5 by ammonia hydroxide. The deposition temperature was 25 °C and the current density was set to 50 mA/cm². Magnetic stirring was utilized to maintain the uniformity of electrolyte. The whole electrodeposition process had a duration of 30 min. Then the samples were taken out, washed with deionized water, dried with compressed air and stored in ambient air for further study. Plasma cleaning was carried out for 8 min using the Plasma Cleaner (Model 1020, Fischione) to quickly remove adsorbed substances on the coating surface with a gas mixture of 25 vol% oxygen and 75 vol% argon.

2.3 Characterisation

Surface morphologies of the Ni-Cu-P ternary coatings were examined by scanning electron microscopy (SEM, JEOL-6490LV) equipped with energy-dispersive X-ray spectroscopy (EDX, INCA, Oxford Instrument Link ISIS-3000) under an acceleration voltage of 20 kV. The phase composition of the coatings was characterized by X-ray diffraction (XRD, Siemens D500) using Cu K α radiation as X-ray source. Surface elements and their binding energy were characterized by an X-ray photoelectron spectroscopy (XPS, Kratos Axis Ultra D1d, Kratos Analytical Limited) using Al K α X-ray as the radiation source and analyzed by CasaXPS software. Hydrophobicity of the surfaces was evaluated using a contact angle

goniometer (FTA200, First Ten Angstroms, Inc.) with water pumping out rate of 1 $\mu\text{L/s}$. The 3D surface topography of coatings was obtained using a 3D Optical Microscope (Contour GT-I, Bruker UK Ltd).

3. Results

3.1 XRD analysis of the coatings

Fig.1 shows the XRD patterns of Ni-based as-deposited coatings before and after plasma cleaning and the stainless steel substrate for comparison. The diffraction patterns for the as-deposited coatings before and after plasma cleaning both have a broad peak at around $44^\circ 2\theta$, which can be attributed to the amorphous phosphorus in as-deposited form [25]. There is also a relatively large, narrower peak at $44.6^\circ 2\theta$, which matches the (111) peak for face-centred cubic Ni at 44.5° (ICDD PDF 00-004-0850), indicating the presence of dominant cubic phase of Ni. The (200) and (220) peaks are not observed, which is likely to be preferably orientated along the (111) plane of Ni grains [26]. The diffraction patterns also contain relatively small peaks at 50.7° and $74.8^\circ 2\theta$. Although these are close to the (200) and (220) peaks of the austenite phase in the substrate, they are broader, indicating the presence of another phase with smaller crystallite size. They could be the (200) and (220) peaks for another face-centred cubic phase, with a lattice parameter of about 3.59 \AA . This is likely to be a solid solution of Cu in Ni, since Ni and Cu can completely dissolve within each other, and the observed lattice parameter is intermediate between those of pure Ni, 3.524 \AA , and pure Cu, 3.615 \AA (ICDD PDF 00-004-0836). Both Ni and Ni-Cu phases remain stable after the plasma cleaning treatment and no new phase appears.

3.2 Surface Morphology of the as-deposited Ni-based coating

Fig.2 (a) and (b) show the secondary electron SEM surface morphology of the as-deposited coating. The surface exhibits regular cauliflower-like hierarchical structure which consists of many tiny spherical deposits that are tightly attached to each other. From the high magnification image, the size of the spherical structures ranges from about 300 nm to 500 nm and size of the cauliflower-like structures is around a few microns. Fig.2 (c) shows the EDX spectrum of the selected area as indicated in Fig.2 (a). There is roughly 60.6 at% nickel, 3.8 at% copper and 4.3 at% phosphorus, which confirms the presence of phosphorus. Fig.2 (d) shows the cross-section image of as-deposited coating surface using backscattered electron. The hierarchical structure can be clearly observed on the coatings. The coating thickness varies from 10 μm to 20 μm due to the high roughness of the surface profile. Fig.2 (e) is the 3D surface topography of the coatings with a selected area of $633 \times 474 \mu\text{m}$. The measured average surface roughness R_a is about $3.91 \pm 0.21 \mu\text{m}$, with many peaks and valleys. The red peaks in the 3D image show the cauliflower structure which is consistent with the SEM observation. The hierarchical structure could provide the desirable specific surface area which will contribute to the improved hydrophobicity.

3.3 Wetting behavior of the Ni-Cu-P ternary coatings

Fig.3 shows the water contact angle (WCA) of the as-deposited coating with different aging durations in the air. The insets show the optical images of the water droplets on the coating surface. The phenomenon could be defined as a time-dependent wetting behavior. It can be seen that the WCA increases gradually from less than 10° to nearly 140° after being aged in ambient air. The change from hydrophilic state to hydrophobic state takes about 60 h. After that, the WCA still increases at a slower rate and stabilises at around 140° .

3.4 XPS analyses of the Ni-Cu-P ternary coatings

Fig.4 compares the high resolution XPS spectra of C 1s (a) and (b) and O 1s (c) and (d) of the as-deposited coating and the coatings stored in air for 10 days, respectively. It can be seen that both C 1s and O 1s spectra changed significantly. To study the details, the C 1s spectra were resolved into several Gaussian-Lorentzian peaks using Shirley backgrounds and the nomenclature proposed by Modabberasl and Skaltsas et al [27, 28]. Specifically, the C 1s satellite peaks were resolved with four different components C=C, C-C/C-H, C-O/C-O-C and COOH/C=O, respectively, in which the hydrocarbon groups (C=C, C-C/C-H) predominate. The peaks were fitted according to the constraint of the intensity ratio between each peak. According to the fitting results, the atomic percentage of hydrocarbon was calculated and shown in Tab.1. The atomic percentage of hydrocarbon increased from 78.7 % (C=C plus C-C/C-H) to 86.5%, while the atomic percentage of the other two C 1s groups decreased from 21.3 % to 13.5 %. The O 1s spectra were also resolved into several constituent satellite peaks, O-Metal which could be designated as lattice oxygen and C-OH and O-H-O groups as non-lattice oxygen identified using the nomenclature proposed by Wei and Khan [29, 30]. The atomic percentage of lattice oxygen decreased from 27.9 % to 14.1 % while the non-lattice oxygen increased from 72.1 % to 85.9 %. The non-lattice oxygen peaks are also attributed to surface adsorbed oxygen species such as hydroxyls or carbonates [31, 32].

3.5 Wetting behavior of Ni-Cu-P ternary coatings with plasma cleaning treatment

Fig.5 shows the WCA change of as-deposited coating before and after plasma cleaning treatment. Plasma cleaning was used to remove the adsorbed substances on the coating surfaces. It is a low energy process without changing the elemental composition and structural characteristics of the coating, and there is no etching or sputtering involved [33]. The as-deposited coating was taken out after plasma cleaning treatment and restored in ambient air. The time-dependent wetting behavior was observed again. It was clearly evidenced that the WCA decreases sharply from over 130° to around 50° after the plasma cleaning. Then the

WCA increased slowly again and nearly recovered to its previous level after a duration of 60 h. The transition from hydrophobic state to hydrophilic state and recovery to hydrophobic state is consistent with the wettability transition of an Ag-coated surface [34]. The initial WCA decrease can be ascribed to the decreasing content of airborne hydrocarbon and increased oxygen groups. The pristine Ni-Cu-P ternary coatings might have high surface energy [35] and present as hydrophilic character. The reason for the later WCA recovery of the coatings can be explained that the hydrocarbon could be re-adsorbed onto the coating surface after being re-exposed to ambient air and the oxygen groups remaining on the coating also decrease. The surface energy was then reduced and the surface hydrophobicity recovered accordingly.

3.6 XPS analyses of the Ni-Cu-P ternary coatings before and after plasma cleaning

Fig.6 shows the high resolution XPS spectra of C 1s (a) and (b) and O 1s (c) and (d) of the as-deposited Ni-based coating before and after plasma cleaning treatment. It clearly indicates that the C 1s contents suffer an obvious decrease. From the resolved peaks, after the plasma cleaning treatment, the atomic percentage of hydrocarbon decrease from 82.3 % (C=C plus C-C/C-H) to 65.9 %, while both the C-O/C-O-C and COOH/C=O groups increase. COOH/C=O works as hydrophilic groups and increases the wettability. This also indicates that the main components of adsorbed airborne hydrocarbon are C-C/C-H groups and C=C groups. For O 1s spectra, there is also a considerable change after plasma cleaning. The lattice-oxygen increased from 10.3 % to 47.8 % while the non-lattice oxygen groups decreased from 89.7 % to 52.2%. The lattice-oxygen included O-Ni and O-Cu groups. The increased oxygen level on the surface may increase the possibility to form hydrogen bonds with interfacial water and lead to lower wettability [30].

4. Discussion

The time-dependent wetting behaviour of the coating appears with the undertaking treatment while the structures and micro-morphologies all remain the same. The possible mechanisms were investigated to interpret this phenomenon.

The wettability of a solid surface is mainly affected by two factors: surface roughness and surface chemistry. Surface roughness plays a crucial role on the wetting behaviour. In the electrodeposition process, cauliflower-like hierarchical coating structure is constructed. The hierarchical structure not only significantly increases the coating surface roughness, but also provides large specific surface area which is desirable for the airborne hydrocarbon adsorption, leading to the driving away of the hydrophilic groups and lowered surface energy [36]. Therefore, a hydrophobic state can be formed gradually.

The changing wettability of Ni-Cu-P ternary coatings would be attributed to the adsorption and re-adsorption process of airborne hydrocarbon and the changing ratio of lattice oxygen on the coating surface, as indicated by the relationship between the WCA and surface carbon and oxygen content over time. The changing wettability may be ascribed to two factors: (i) adsorption of airborne hydrocarbon and (ii) influence of lattice oxygen.

Firstly, the XPS analysis shows that the amount of hydrocarbon groups present on the surface is indeed increasing with exposure time, indicating that hydrocarbons are adsorbed onto the coating surface in ambient air. As shown in Fig.7, the surface carbon content changes significantly. The highly rough cauliflower surface structure could provide greater specific surface area than a smooth surface, which is easier for airborne hydrocarbon to be adsorbed. The surface carbon increases from less than 20 at% to around 35 at%. The increased carbon content is attributed to the physisorption of airborne hydrocarbons, which include C=C and C-C/C-H groups. They could then form a thin layer on the coatings, leading to lower surface energy [37]. The atomic ratio of the airborne hydrocarbon increases with time, as shown in

Tab.1, which indicates that partial adsorption [33] of these groups was undergone on the Ni-Cu-P ternary coating surface. This may also have led to the continuous decrease of surface energy over time. Similar phenomena have been reported for a variety of metal oxide materials including zirconium dioxide (ZrO_2) and titanium dioxide (TiO_2) [35, 38]. In the present work, van-der-Waals and hydrogen bonding are the two typical bonding, besides possible electrovalent bonding of Ni-O and Cu-O [39]. The mechanism for this relationship can be explained by considering the adsorbed hydrocarbons as hydrophobic defects on hydrophilic surface [40]. A hydrocarbon molecule would diffuse along the surface, and the van der Waals bonding between the surface and the adsorbed hydrocarbon could help to increase the stability of the studied coating systems. Hence, the diffusion of hydrocarbon molecules is likely to occur. After the plasma cleaning, the WCA decreases with the removal of adsorbed hydrocarbon, which is also consistent with the decreased surface carbon content shown in Fig. 7. This could explain the reason for time-dependent wetting behavior.

The second factor, the changing oxygen groups may also contribute to the change of surface wettability change observed. Excess lattice oxygen and hydroxyl groups may exist on the surface after the electrodeposition. And the surface lattice oxygen could be released during the following long-time exposure to ambient air. The lattice oxygen could be desorbed from the surface and the surface hydrocarbons also work in conjunction with the incident photon energy to release oxygen from the coating lattice [41]. With the extensive surface relaxation, less lattice oxygen remains. Such process may also contribute to the coatings surface transition from hydrophilic to hydrophobic, while the main reason could be the notable change in surface carbon content. After the plasma cleaning, with the removal of the adsorbed hydrocarbon, the increased lattice oxygen (O-Metal) makes it easier to form hydrogen bonds with interfacial water on the surface [30, 42]. Hydrophilic groups such as hydroxyls could also be introduced onto the surface during the process, which also benefits the increase of the surface energy.

Similar time-dependent phenomenon was also observed on other electrodeposited coatings produced with different current densities as shown in Fig. 8. The WCA shows the same changing trends which indicates that the time-dependent wetting behavior could be a common phenomenon. The reason for the different WCAs after plasma cleaning could be the surface roughness difference of different coating surfaces.

In summary, the changing wettability of Ni-Cu-P ternary coating is a combined result of airborne hydrocarbon adsorption and lattice oxygen variation. The adsorption of airborne hydrocarbon takes the major effect, while the lattice oxygen on the coating surface also influences the surface wettability.

Herein, the time-dependent wetting behaviour could be clearly explained by the schematic diagram in Fig. 9. There are very limited hydrocarbons adsorbed on the as-deposited coating surface, which presents a hydrophilic state. After stored in ambient air, a great amount of hydrocarbons are adsorbed onto the coating surface, which reduces the surface energy significantly and turns the surface into a hydrophobic wetting state.

5. Conclusions

Ni-Cu-P ternary coating with hierarchical structure was prepared using electrodeposition method on 304 SS substrates. It was found that the surface of the as-deposited coatings changed from hydrophilic state to hydrophobic state after aging in ambient air. This time-dependent wetting behavior was investigated with the assistance of plasma cleaning to study the possible surface adsorption contributing to the time-dependent wetting behavior. The main reason for the changing wetting behavior could be ascribed to the adsorption of airborne hydrocarbon and the change of lattice oxygen. The two factors altered the surface energy and introduce more hydrophobic groups onto the coating surface, resulting in the changes of wetting behavior. This study provides insight into the wetting mechanism of the metallic

materials and highlights the importance of controlling hydrocarbon adsorption for material wetting behavior.

Acknowledgments: The work is supported by a joint Ph.D. studentship between China Scholarship Council (CSC) and The University of Nottingham. The authors acknowledge the use of facilities at Nanoscale and Microscale Research Centre of the University of Nottingham.

References

- [1] L. Bocquet, E. Lauga, A smooth future? *Nature materials*, 10 (2011) 334.
- [2] X. Deng, L. Mammen, H.-J. Butt, D. Vollmer, Candle soot as a template for a transparent robust superamphiphobic coating, *Science*, 335 (2012) 67-70.
- [3] H. Liu, P. Zhang, M. Liu, S. Wang, L. Jiang, Organogel-based Thin Films for Self-Cleaning on Various Surfaces, *Advanced Materials*, 25 (2013) 4477-4481.
- [4] J. Jia, J. Fan, B. Xu, H. Dong, Microstructure and properties of the super-hydrophobic films fabricated on magnesium alloys, *Journal of Alloys and Compounds*, 554 (2013) 142-146.
- [5] J. Liu, Z.A. Janjua, M. Roe, F. Xu, B. Turnbull, K.-S. Choi, X. Hou, Superhydrophobic/icephobic coatings based on silica nanoparticles modified by self-assembled monolayers, *Nanomaterials*, 6 (2016) 232.
- [6] L. Shi, J. Hu, X. Lin, L. Fang, F. Wu, J. Xie, F. Meng, A robust superhydrophobic PPS-PTFE/SiO₂ composite coating on AZ31 Mg alloy with excellent wear and corrosion resistance properties, *Journal of Alloys and Compounds*, 721 (2017) 157-163.
- [7] J. Ou, W. Hu, S. Liu, M. Xue, F. Wang, W. Li, Superoleophobic textured copper surfaces fabricated by chemical etching/oxidation and surface fluorination, *ACS applied materials & interfaces*, 5 (2013) 10035-10041.
- [8] S.G. Dieter't Mannetje, R. Lagraauw, S. Otten, A. Pit, C. Berendsen, J. Zeegers, D. Van Den Ende, F. Mugele, Trapping of drops by wetting defects, *Nature communications*, 5 (2014).
- [9] M. Tang, V. Shim, Z. Pan, Y. Choo, M. Hong, Laser ablation of metal substrates for superhydrophobic effect, *Journal of Laser Micro/Nanoengineering*, 6 (2011) 346-352.
- [10] C. Mrabet, R. Dridi, N. Mahdhi, M. Amlouk, Mechanism of wettability conversion on sprayed Zn₂SnO₄ thin films surfaces modified by thermal annealing in air, *Journal of Alloys and Compounds*, 725 (2017) 765-772.
- [11] T. Verho, C. Bower, P. Andrew, S. Franssila, O. Ikkala, R.H. Ras, Mechanically durable superhydrophobic surfaces, *Advanced Materials*, 23 (2011) 673-678.

- [12] V. Kondrashov, J.r. Rhe, Microcones and nanograss: toward mechanically robust superhydrophobic surfaces, *Langmuir*, 30 (2014) 4342-4350.
- [13] Y. Wei, L. Hongtao, Z. Wei, Preparation of anti-corrosion superhydrophobic coatings by an Fe-based micro/nano composite electro-brush plating and blackening process, *RSC Advances*, 5 (2015) 103000-103012.
- [14] S. Khorsand, K. Raeissi, F. Ashrafizadeh, M.A. Arenas, Super-hydrophobic nickel–cobalt alloy coating with micro-nano flower-like structure, *Chemical Engineering Journal*, 273 (2015) 638-646.
- [15] A. Vorobyev, C. Guo, Multifunctional surfaces produced by femtosecond laser pulses, *Journal of Applied Physics*, 117 (2015) 033103.
- [16] M. Palaniappa, S.K. Seshadri, Friction and wear behavior of electroless Ni–P and Ni–W–P alloy coatings, *Wear*, 265 (2008) 735-740.
- [17] J.N. Balaraju, K.S. Rajam, Electroless deposition of Ni–Cu–P, Ni–W–P and Ni–W–Cu–P alloys, *Surface and Coatings Technology*, 195 (2005) 154-161.
- [18] Y. Liu, Q. Zhao, Study of electroless Ni–Cu–P coatings and their anti-corrosion properties, *Applied Surface Science*, 228 (2004) 57-62.
- [19] Y. Xu, X. Zheng, X. Hu, Y. Yin, T. Lei, Preparation of the electroless Ni–P and Ni–Cu–P coatings on engine cylinder and their tribological behaviors under bio-oil lubricated conditions, *Surface and Coatings Technology*, 258 (2014) 790-796.
- [20] D.-D. Kupferinstitut, Legierungen des Kupfers mit Zinn, Nickel, Blei und anderen Metallen, in, Berlin–Dsseldorf, 1965.
- [21] W. Zhang, H. Cao, X. Feng, A. Hu, M. Li, Structure and wettability control of Cu–Ni–P alloy synthesized by electroless deposition, *Journal of Alloys and Compounds*, 538 (2012) 144-152.
- [22] C.-J. Chang, S.-T. Hung, Wettability control of micropore-array films by altering the surface nanostructures, *Journal of nanoscience and nanotechnology*, 10 (2010) 4674-4678.
- [23] V.A. Dhumale, P.V. Shah, I. Mulla, R. Sharma, Switching of hydrophilic to ultra hydrophilic properties of flower-like gold nanostructures, *Applied Surface Science*, 256 (2010) 4192-4195.
- [24] P. Liu, L. Cao, W. Zhao, Y. Xia, W. Huang, Z. Li, Insights into the superhydrophobicity of metallic surfaces prepared by electrodeposition involving spontaneous adsorption of airborne hydrocarbons, *Applied Surface Science*, 324 (2015) 576-583.

- [25] Q.X. Mai, R.D. Daniels, H.B. Harpalani, Structural changes induced by heating in electroless nickel-phosphorus alloys A2-Krutenat, R.C, in: Metallurgical Coatings 1988, Elsevier, 1988, pp. 235-247.
- [26] R. Ashiri, Analysis and characterization of phase evolution of nanosized BaTiO₃ powder synthesized through a chemically modified sol-gel process, Metallurgical and Materials Transactions A, 43 (2012) 4414-4426.
- [27] T. Skaltsas, X. Ke, C. Bittencourt, N. Tagmatarchis, Ultrasonication Induces Oxygenated Species and Defects onto Exfoliated Graphene, The Journal of Physical Chemistry C, 117 (2013) 23272-23278.
- [28] A. Modabberasl, P. Kameli, M. Ranjbar, H. Salamati, R. Ashiri, Fabrication of DLC thin films with improved diamond-like carbon character by the application of external magnetic field, Carbon, 94 (2015) 485-493.
- [29] W. Wei, X. Cui, W. Chen, D.G. Ivey, Phase-controlled synthesis of MnO₂ nanocrystals by anodic electrodeposition: implications for high-rate capability electrochemical supercapacitors, The Journal of Physical Chemistry C, 112 (2008) 15075-15083.
- [30] S. Khan, G. Azimi, B. Yildiz, K.K. Varanasi, Role of surface oxygen-to-metal ratio on the wettability of rare-earth oxides, Applied Physics Letters, 106 (2015) 061601.
- [31] L. Martinez, E.d. Roman, J. De Segovia, S. Poupard, J. Creus, F. Pedraza, Surface study of cerium oxide based coatings obtained by cathodic electrodeposition on zinc, Applied Surface Science, 257 (2011) 6202-6207.
- [32] J. Fan, X. Wu, L. Yang, D. Weng, The SMSI between supported platinum and CeO₂-ZrO₂-La₂O₃ mixed oxides in oxidative atmosphere, Catalysis Today, 126 (2007) 303-312.
- [33] B. Willems, A.-L. Hamon, D. Schryvers, A.C. Robins, J.M. Matesa, P.E. Fischione, Plasma cleaning of carbonaceous samples using a shield, Microsc. Microanal, 9 (2003) 164.
- [34] L. Sheng, W. Fajun, L. Wen, Q. Guanjun, Reversible wettability between superhydrophobicity and superhydrophilicity of Ag surface, Science China Materials, 59 (2016) 348-354.
- [35] D.J. Preston, N. Miljkovic, J. Sack, R. Enright, J. Queeney, E.N. Wang, Effect of hydrocarbon adsorption on the wettability of rare earth oxide ceramics, Applied Physics Letters, 105 (2014) 011601.
- [36] R. Ashiri, A mechanistic study of nanoscale structure development, phase transition, morphology evolution, and growth of ultrathin barium titanate nanostructured films, Metallurgical and Materials Transactions A, 45 (2014) 4138-4154.

- [37] D.L. Katz, W. Saltman, Surface tension of hydrocarbons, *Industrial & Engineering Chemistry*, 31 (1939) 91-94.
- [38] S. Takeda, M. Fukawa, Y. Hayashi, K. Matsumoto, Surface OH group governing adsorption properties of metal oxide films, *Thin Solid Films*, 339 (1999) 220-224.
- [39] J.-H. Kim, J. Jung, K. Tahara, Y. Tobe, Y. Kim, M. Kawai, Direct observation of adsorption geometry for the van der Waals adsorption of a single π -conjugated hydrocarbon molecule on Au (111), *The Journal of chemical physics*, 140 (2014) 074709.
- [40] R. Raj, R. Enright, Y. Zhu, S. Adera, E.N. Wang, Unified model for contact angle hysteresis on heterogeneous and superhydrophobic surfaces, *Langmuir*, 28 (2012) 15777-15788.
- [41] Y. Shapira, S. Cox, D. Lichtman, Chemisorption, photodesorption and conductivity measurements on ZnO surfaces, *Surface Science*, 54 (1976) 43-59.
- [42] S. Granick, S.C. Bae, A curious antipathy for water, *Science*, 322 (2008) 1477-1478.

CAPTIONS

Figure 1 XRD patterns of 304 SS and the Ni-Cu-P ternary coatings

Figure 2 SEM images of surface morphologies (a) and (b) EDX results (c) Cross-section morphology (d) and 3D image (e) of the as-deposited Ni-Cu-P ternary coating

Figure 3 WCA change within exposure time in ambient air of the as-deposited Ni-Cu-P ternary coating

Figure 4 (a) and (b) C 1s XPS spectrum of the Ni-Cu-P composite coating (a) As-deposited (b) After 10 days (store in ambient air); (c) and (d) O 1s XPS spectrum of the Ni-Cu-P ternary coating (c) As-deposited (d) After 10 days (store in ambient air)

Figure 5 WCA change of Ni-Cu-P ternary coating before and after plasma cleaning treatment

Figure 6 (a) and (b) C 1s XPS spectrum of the Ni-Cu-P ternary coating (a) before (b) after plasma cleaning treatment; (c) and (d) O 1s XPS spectrum of the Ni-Cu-P ternary coating (c) before (d) after plasma cleaning treatment

Figure 7 Surface carbon content evolution versus different treatments

Figure 8 WCA changes of Ni-Cu-P coatings before and after plasma cleaning treatment with different deposition current density (a) 50 mA/cm² (b) 100 mA/cm² (c) 150 mA/cm²

Figure 9 Schematic of the time-dependent wetting behaviour of the Ni-Cu-P coating

Table 1 The atomic percent change of hydrocarbon groups and lattice oxygen groups versus different treatments

CAPTIONS for Supplemental Materials

Figure S1. Step-wise flowchart of the coating preparation

Figure S2. Water contact angle images of Ni-Cu-P ternary coating at different stages: (a) as-deposited (b) After stored in air for 10 days (c) 0.5 h after Plasma cleaning treatment (d) Restored in air for 54.5 h after plasma cleaning treatment

Figure S3. 3D images of the as-deposited Ni-Cu-P ternary coating (a) before and (b) after plasma cleaning treatment.

Figure S4. SEM image with different magnifications of the as-deposited Ni-Cu-P ternary coating: (a) × 100 (b) × 300 (c) × 500 and (d) × 1000

Figure S5. SEM image with low magnifications of cross-section area of the as-deposited Ni-Cu-P ternary coating: (a) × 500 and (b) × 1000.

Tab.1

Concentration At%	As- deposited	After 10days	Before Plasma cleaning (After 30 days)	After Plasma Cleaning
Hydrocarbon in all (%)	78.7	86.5	82.3	65.9
Lattice Oxygen (%)	27.9	14.1	10.3	47.8

Figure 1

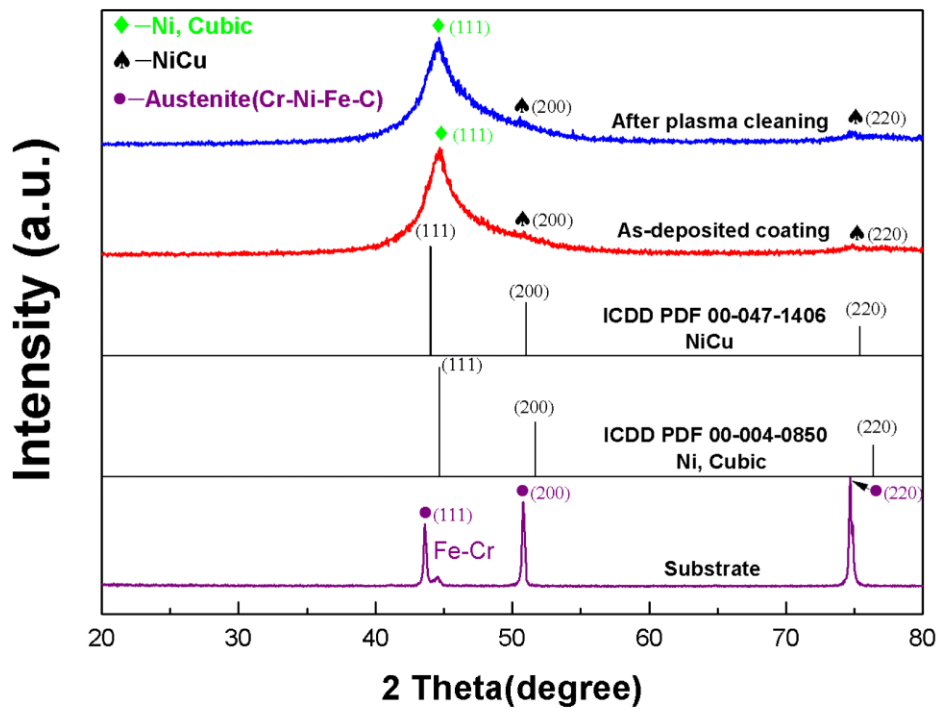


Figure 2

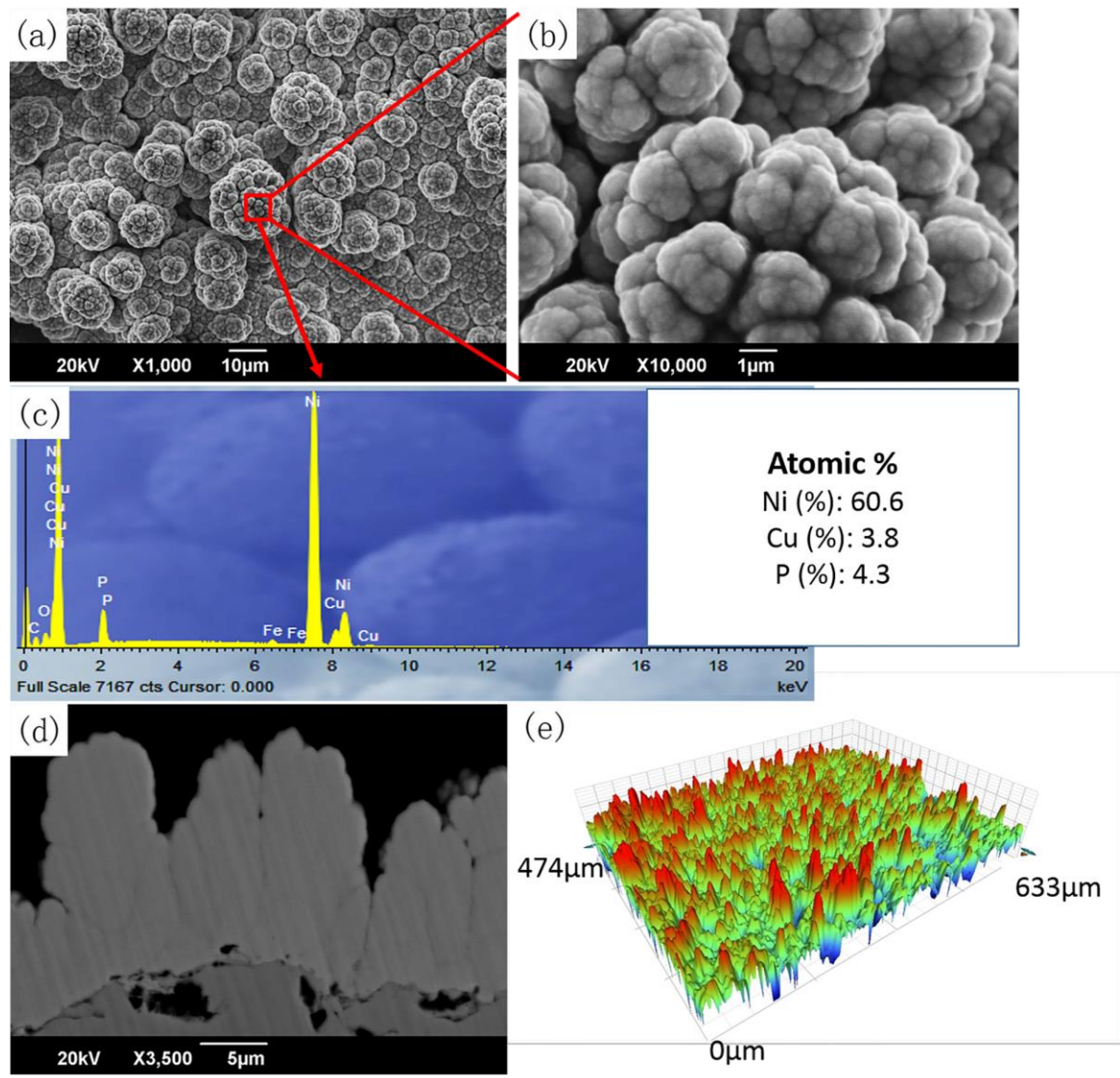


Figure 3

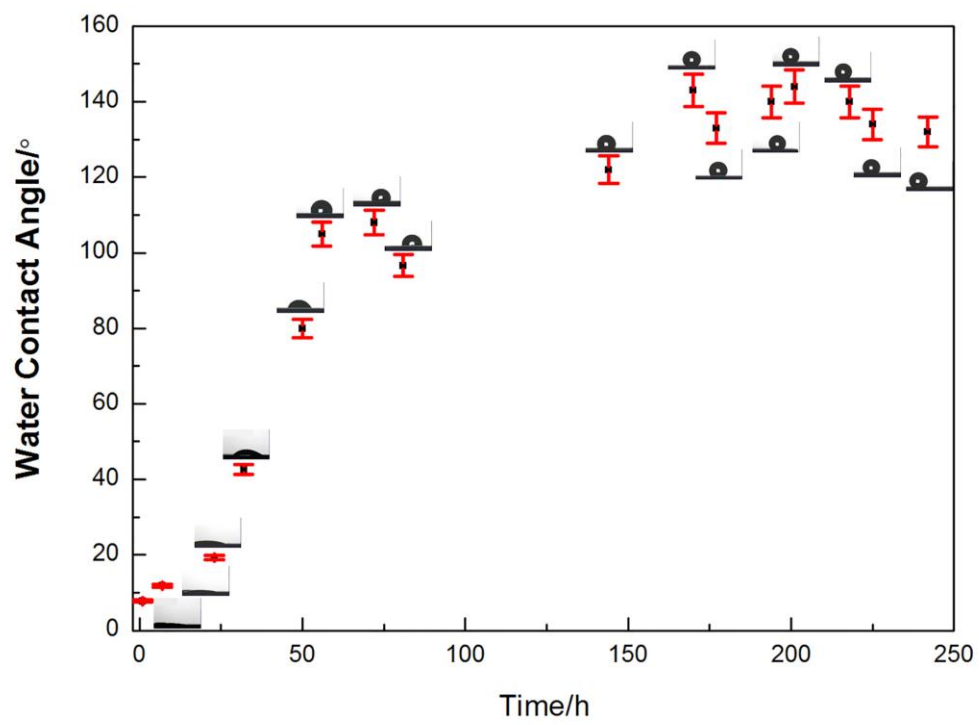


Figure 4

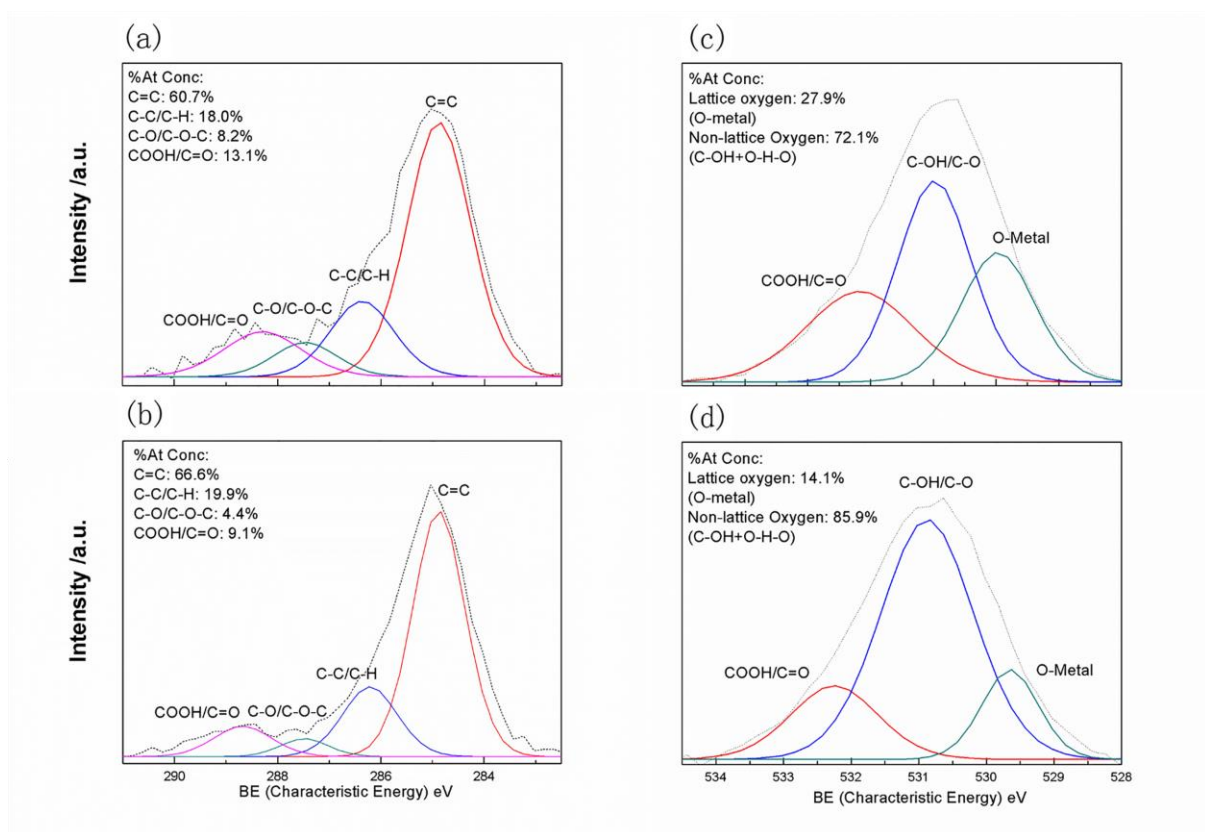


Figure 5

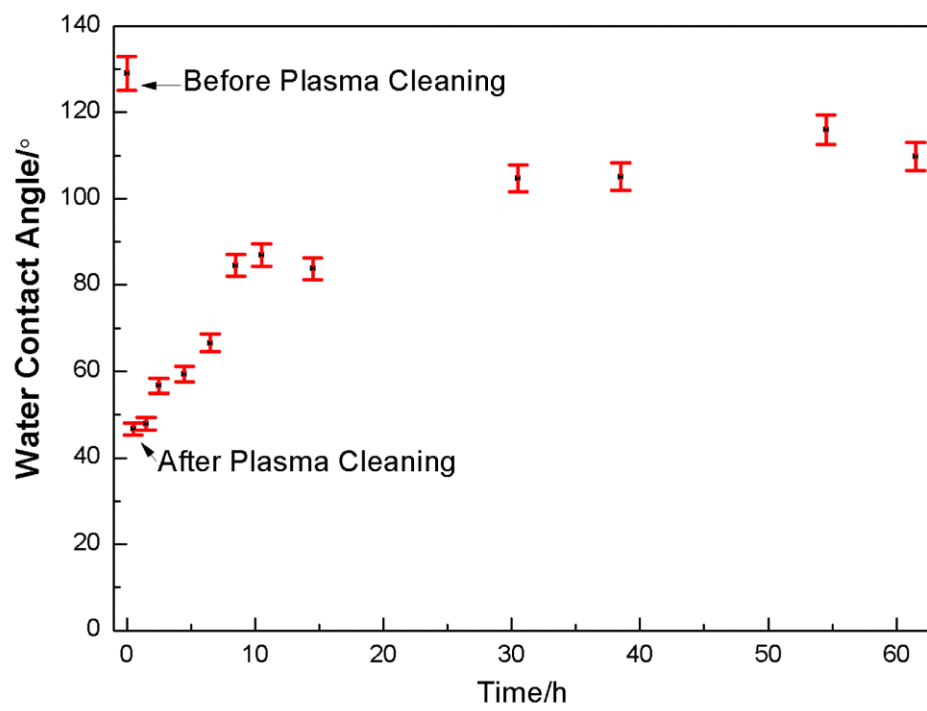


Figure 6

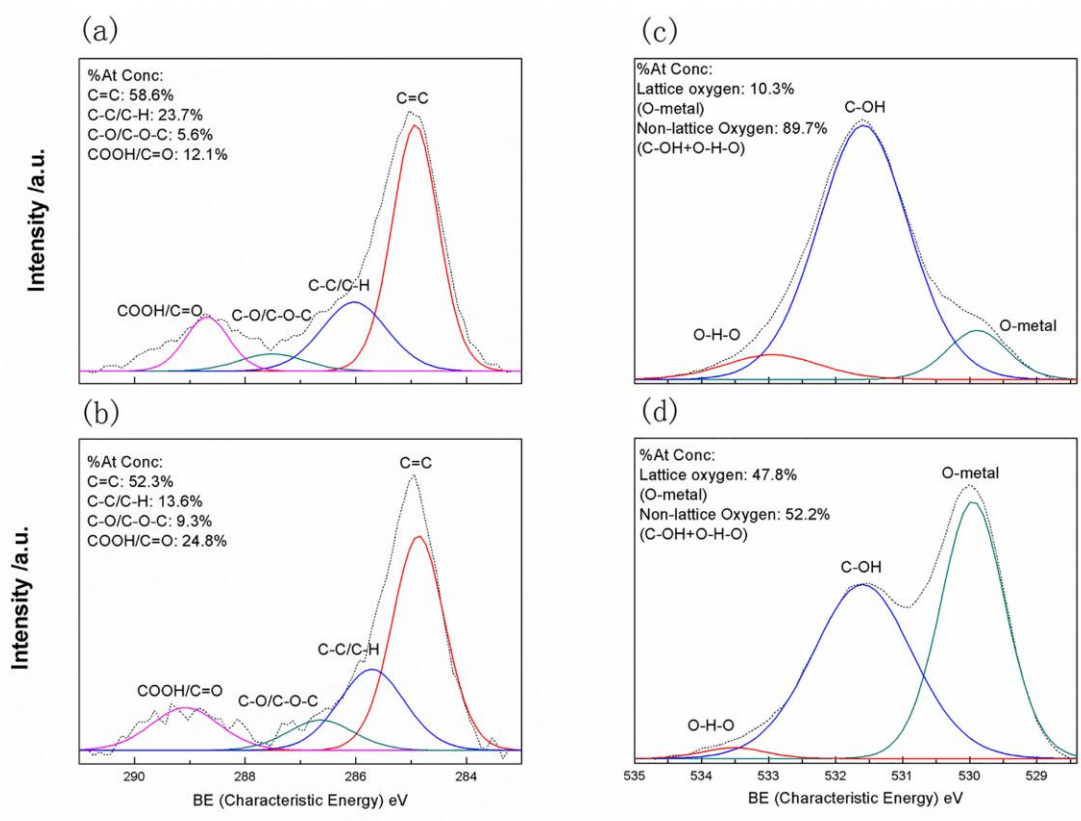


Figure 7

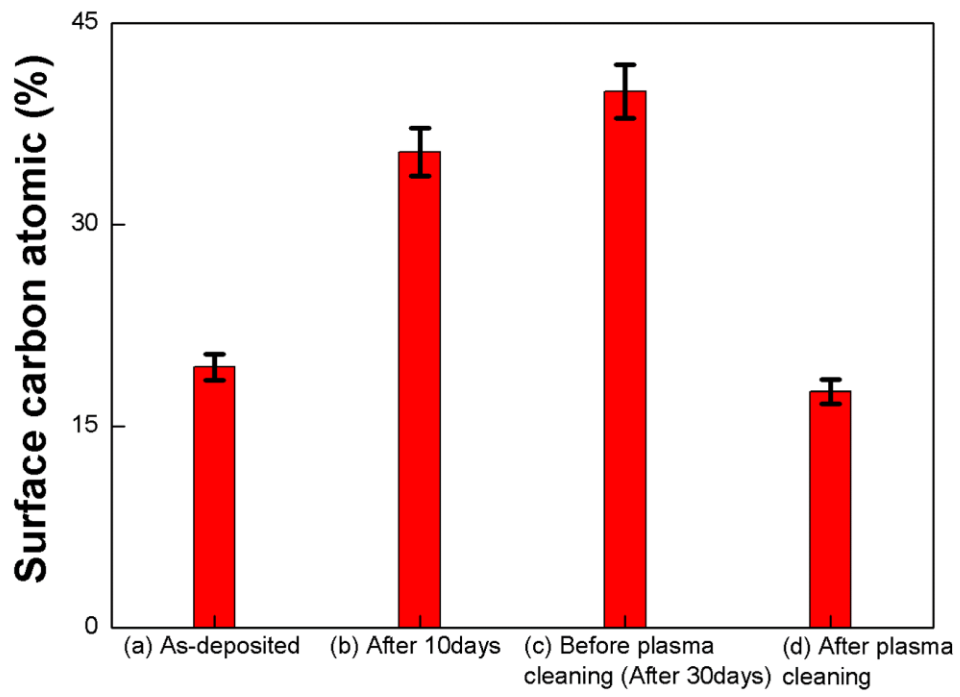


Figure 8

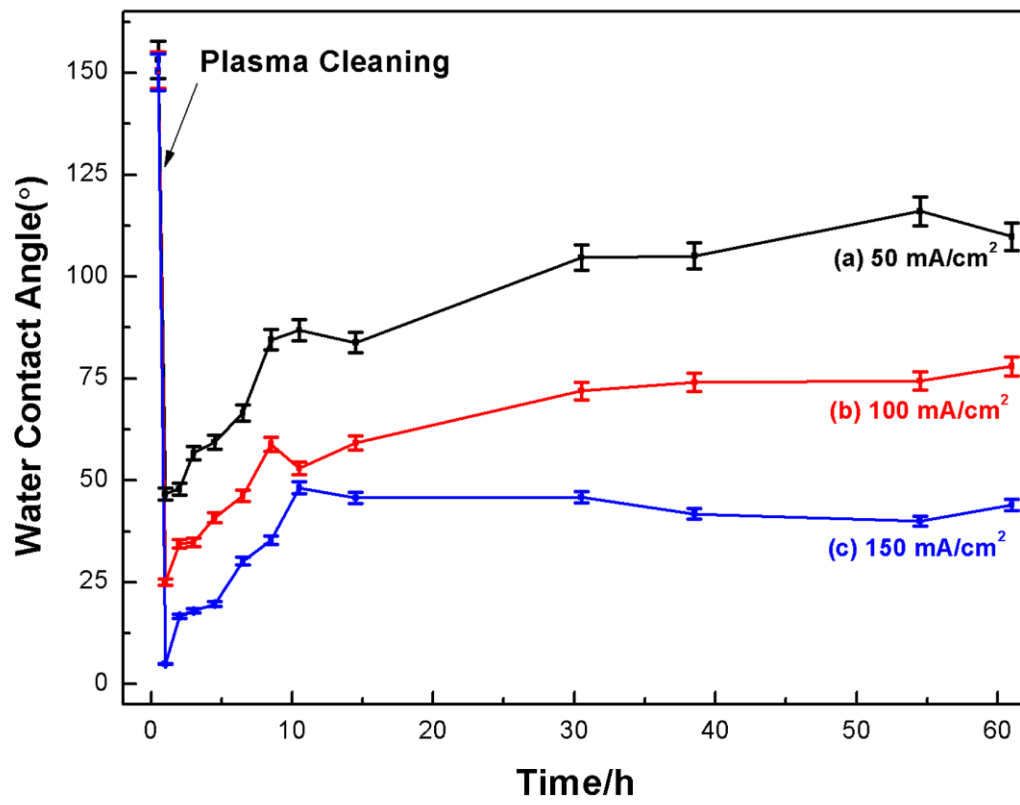


Figure 9

